Surface & Coatings Technology 525 (2026) 133317

Contents lists available at ScienceDirect

Surface & Coatings Technology

journal homepage: www.elsevier.com/locate/surfcoat

Friction and galling reduction potential of Ni-Ag-MoS_2 coating by laser metal deposition at intermediate temperatures

B. Podgornik [a,b,*], V. Yarasu [a], B. Šetina Batič [a], M. Rodriguez Ripoll [c]

[a] Institute of Metals and Technology, Lepi pot 11, 1000, Ljubljana, Slovenia
[b] Faculty of Industrial Engineering, Šegova ul. 112, Novo mesto, Slovenia
[c] AC2T research GmbH, Viktor-Kaplan Strasse 2/C, 2700, Wiener Neustadt, Austria

ARTICLE INFO

Keywords:
Laser metal deposition
Galling
Hot forming
Solid lubricant
Friction

ABSTRACT

Galling is a critical limitation in high-temperature forming of corrosion resistant and light-weight alloys such as austenitic stainless steel, aluminum, and titanium, as conventional lubricants rapidly degrade. This study investigates the anti-galling potential of a Ni-based self-lubricating alloy containing Ag and MoS_2, applied by laser metal deposition. The coating performance was benchmarked against conventional hot work tool steel using a load-scanning tribometer at room temperature and 150–300 °C against AA6082 aluminum alloy, AISI 316L austenitic stainless steel, and Ti6Al4V titanium alloys.

The investigated Ni-based coating containing Ag and MoS_2 although not being able to completely eliminate use of solid lubricant in mid-temperature range, it provided markedly improved tribological behavior compared to reference tool steel. Against AA6082 and AISI 316L, friction was reduced by up to 50%, galling initiation loads increased by about 30%, and adhered counter-body material was suppressed by up to 60%. At elevated temperatures (150–300 °C), synergistic in-situ formation of Ag_2S, Cr_2S_3/Cr_3S_4, and Cr_2O_3 tribo-compounds on the contact surface effectively delayed work-material adhesion and transfer layer build-up. For Ti6Al4V, galling could not be completely avoided, but it was mitigated via thinner and more discontinuous transfer layers when using the Ni-based laser metal deposited coating, particularly at 300 °C. Multicycle tests confirmed extended stability of low-friction regimes and reduced accumulation of adhered material.

These findings highlight that Ni-Ag-MoS_2 coatings deposited by laser metal deposition provide significant improvements in galling resistance and friction control, offering a promising route to extend tool life and reduce reliance on external lubricants in hot forming of corrosion resistant and light-weight structural alloys.

1. Introduction

A major challenge in high-temperature forming is transfer and adhesion of counterbody material to the tool surface, known as galling [1,2]. This is especially problematic in the case of high-strength, light-weight and corrosion resistant alloys (i.e. stainless steel, aluminum and titanium alloys) which are very prone to galling. Adhesive wear and galling can be effectively prevented by the use of lubricants. They do not only reduce tool wear but also provide low and stable friction, thus resulting in better surface quality of produced parts. However, the use of forming oils and greases in forming applications involves possible environmental and health hazards, additional cleaning steps and increased costs related to their recycling and disposal [3]. Some of those issues can be avoided by using vegetable-based lubricants, which however show reduced performance in demanding forming applications with a high degree of plastic deformation. Oils and greases, especially vegetable-based have another significant limitation. They cannot be used in high-temperature forming applications as they quickly thermally degrade at elevated temperatures [4]. For high-temperature forming applications solid lubricants like graphite, MoS_2 and hexagonal boron nitride (hBN) are commonly applied [5,6]. They provide low and stable friction and prevent galling, but need constant re-application and deposition, cause environment, process and equipment contamination, as well as require demanding cleaning of the equipment and parts [6,7]. Last but not least, they can also result in air-born dust particles that pose potential health hazards to operators.

Another approach for improving tool wear and galling resistance is the application of hard-coatings. Different types of coatings have been

* Corresponding author at: Institute of Metals and Technology, Lepi pot 11, 1000, Ljubljana, Slovenia.
E-mail address: bojan.podgornik@imt.si (B. Podgornik).

https://doi.org/10.1016/j.surfcoat.2026.133317
Received 3 February 2026; Received in revised form 17 February 2026; Accepted 17 February 2026
Available online 19 February 2026

developed, tested and applied in forming processes. The most common are hard PVD Ti- and Cr-based coatings [4]. However, they require high-performance tool-steel substrate material with excellent load-carrying capacity and very smooth surface. Their thickness is limited to few microns and is very hard to be uniformly deposited on complex shapes, as typically found in forming tools. However, their main limitation is related to relatively high friction and galling tendency against soft metals [8,9]. To overcome problem of high friction and adhesion hard ceramic coatings can be combined with top diamond like carbon (DLC) coatings or by adding vanadium (i.e. CrVN, TiVCN, AlCrVN, …), which forms lubricious oxides or Magneli phases at elevated temperatures [10]. However, while DLC coatings may degrade and start losing their wear resistance and properties at temperatures above 150 °C [8], V-containing coatings need much higher temperatures, above 600 °C to form lubricious oxides and provide self-lubricating properties [10,11]. V-based compounds may also pose health risks due to their toxicity [12].

In recent years self-lubricating laser metal deposited coatings or laser-claddings capable of operating at temperatures well above 300 °C are subject of growing interest and research within the field of hot forming [13–15]. Laser-claddings can be effectively used for the single-pass deposition of thick wear protective coatings on cheap and easily available simple substrate materials. These coatings also show good quality and density, excellent metallurgical bonding to the substrate, as well as refurbishing capability [16]. Ni-based alloys have been found as the most suitable base materials for laser-claddings in high-temperature applications [17]. Self-lubricating properties in a broad temperature range are further achieved through addition of solid materials with low shear strength and toughness. These can include different soft metals like coper, silver and gold, metal oxides (i.e. CaO, NiO) and transition metal dichalcogenides (i.e. MoS_2, WS_2, …) [6]. However, each lubrication phase has a different activation and operation temperature range, which requires combination of different phases for good self-lubricating performance. Combination of silver and MoS_2 has been subject of many investigations and found as a good combination for high-temperature applications [14,18,19]. Silver is an effective solid lubricant at high temperatures with high thermal conductivity. Its lubrication capability is based upon its low shear strength and diffusion to sliding surface at high temperatures [5,6,20]. On the other hand, MoS_2 lubrication is based on its layered microstructure with the layers aligning in the direction of motion and providing low friction up to temperature of 400 °C [5,6]. The combination of Ag and MoS_2 can also lead to the in-situ formation of lubricious silver molybdates, such as Ag_2MoO_4 and $Ag_2Mo_2O_7$ at temperatures between 500 and 600 °C [21,22].

Although several Ni-based self-lubricating claddings have been the subject of interest and research in recent years, those investigations are mainly focused on phases characterization, identification of lubrication mechanisms and performance at temperatures above 400 °C, mostly relying on simple pin-on-disc sliding tests [17–22]. The aim of the present investigation is to evaluate friction reducing potential of a Ni-based laser metal deposited coating incorporating Ag-MoS_2 solid lubricant at intermediate temperatures (150–300 °C), and focusing on galling resistance under representative forming conditions against alloys that are particularly prone to adhesive wear and galling.

2. Experimental

2.1. Materials and coatings

Ni-based coating used in this investigation, already extensively examined by H. Torres et al. [22] was deposited via laser metal deposition using a high-power direct diode laser system (HighLight D8000) operating at a wavelength of 975 nm. A commercial Ni-based self-fluxing alloy (NiCrSiB, Castolin Eutectic) was used as the temperature resistant matrix powder, with a particle size of 50–150 μm and a nominal composition (wt%): 0.2% C, 4.0% Cr, 2.5% Si, 1.0% B, <2.0% Fe, 1.0% Al, balance Ni. The additions of boron and silicon effectively lower the alloy's melting point, enhancing processability and promoting deposition of dense, defect-free coatings [23]. To enhance tribological performance under elevated-temperature conditions, 5 wt% silver (Goodfellow, ≤45 μm) and 10 wt% molybdenum disulfide (Tribotecc GmbH, 5–75 μm) were added as solid lubricant precursors. This specific combination was previously identified by H. Torres and authors [22] as optimal in terms of microstructure, solid lubricants distribution across the coating, hot hardness, and high-temperature oxidation resistance.

The powder blend was homogenized by mechanical mixing with ethanol as a temporary binder. The resulting slurry was uniformly spread onto sandblasted AISI 304 (1.4301) stainless steel plates with a hardness of 150 HV. AISI 304 was selected as a substrate material due to its good oxidation resistance, low cost, and ease of machining. The coated plates were then dried in an oven at 100 °C for 1 h to remove residual ethanol. Laser metal deposition was performed under a single-pass/single-layer configuration under a protective argon atmosphere to prevent coating re-melting and oxidation. A rectangular laser beam of 24 × 3 mm^2 was used, combined with a laser scan speed of 10 mm/s, power density of approx. 85 W/mm^2 and energy input of 10 J/mm^3. After laser metal deposition, the coated plates with a coating thickness of about 5 mm were machined longitudinally into Ø 10 mm × 100 mm cylinders, with a cladded surface covering approximately one-third of the cylinder's cross-section (Fig. 1). This sector was used as the sliding contact zone in tribological testing. Final surface preparation included grinding and polishing of the cylinders to a surface roughness Ra ≈ 0.15 μm.

The coating exhibited a room-temperature hardness of 385 HV and retained 360–330 HV at temperatures between 150 °C and 300 °C. It has typical dendritic microstructure with aggregates of up to 50 μm in size spread across the entire thickness of the coating, which is consistent with already published results [22]. The microstructure and chemical composition of the deposited Ni–5Ag–10MoS_2 coating have been extensively characterized, presented and discussed in detail in Refs. [14,22], including XRD and EBSD measurements. Therefore, only representative OM and SEM images of the as-deposited microstructure are shown in Fig. 2. Matrix composition as measured by spot EDS away from the aggregates was (in wt%) 89.7 ± 1.1% Ni, 3.9 ± 0.2% Cr, 3.1 ± 0.3% Si, 1.6 ± 0.4% Fe, 1.7 ± 0.2% Al. The main crystallographic phases for the load carrying matrix material are Ni-borides (Ni_2B and Ni_3B) and Ni-based solid solution. On the other hand, aggregates are composed of bright, globular inclusions (spot A, Fig. 2b) surrounded by dark phase (spot B, Fig. 2b). The bright phase is composed predominantly of elemental silver and encapsulated within chromium- and sulfur-rich dark phase. Dark phase mainly consists of a mixture of chromium sulfides (CrS and Cr_3S_4) arising from the thermal decomposition of MoS_2 during laser metal deposition [14,24] and occasional small fractions of MoS_2, possibly being re-formed during sample cooling. Additionally, presence of nickel sulfides such as NiS_2 and Mo-carbides (spot C, Fig. 2b), also originating from MoS_2 decomposition, has also been identified and observed within the matrix [14]. It must be noted that both silver and the aforementioned chromium sulfides have been described in the available literature as effective high temperature lubricants [25].

For benchmarking, a high-performance ESR hot work tool steel QRO 90 Supreme from Uddeholm (HWTS-QRO) was used as the reference material. Its nominal chemical composition is (in wt%): 0.38% C, 0.3% Si, 0.75% Mn, 2.6% Cr, 2.25% Mo, 0.9% V, balance Fe. The steel was heat treated according to the supplier's recommended procedure (quenching and double tempering), yielding a microstructure of tempered martensite with a dense distribution of small, finely dispersed alloying carbides of MC and M_2C type (Fig. 3), and final hardness of 540 HV. After heat treatment cylindrical specimens were ground and polished to an average surface roughness (R_a) of 0.15 μm.

Three commonly used alloys, each known to exhibit high galling susceptibility during high-temperature forming, were chosen as counter-body materials. These included AISI 316L stainless steel (SS) in solution-

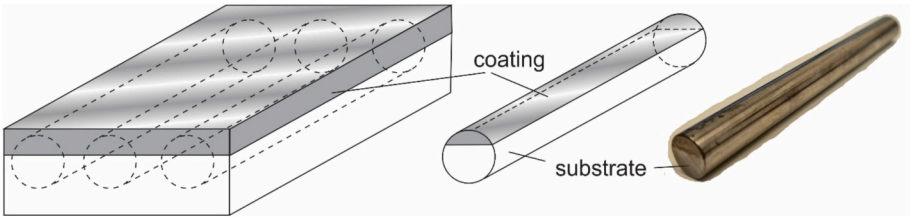

Fig. 1. Preparation of test cylinders with a laser metal deposited Ni–5Ag–10MoS_2 coating.

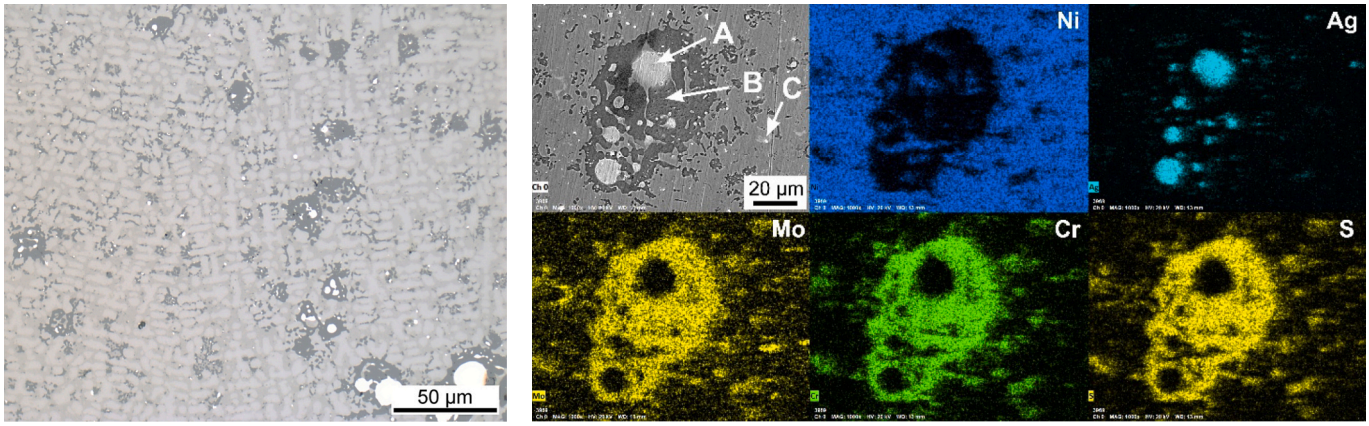

Fig. 2. Typical microstructure of Ni-5Ag-10MoS_2 coating; (a) OM and (b) SEM with EDS mapping (cf. [22]).

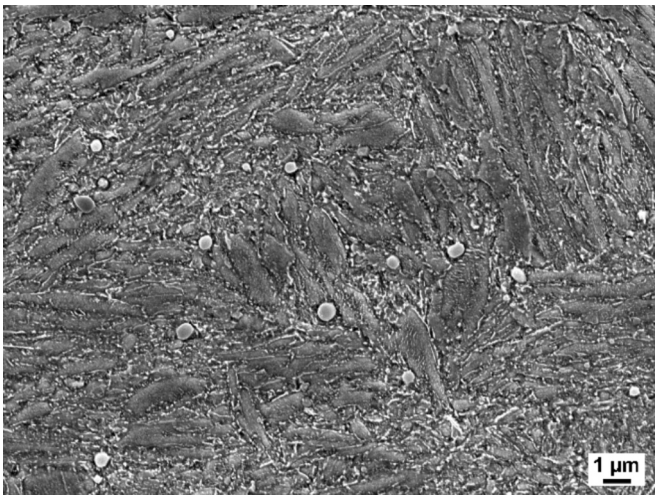

Fig. 3. Microstructure of reference hot work tool steel (HWTS-QRO).

annealed condition (hardness 270 HV), wrought AA6082 Al-Mg-Si aluminum alloy in T6 temper condition (solution heat treatment and artificial aging, hardness 115 HV) commonly used in highly stressed applications and the most common titanium alloy Ti6Al4V in annealed condition (hardness 300 HV). All counter-body materials were machined into Ø10 mm × 100 mm cylinders, followed by surfaces grinding and polishing to achieve a uniform surface roughness (R_a) of 0.2–0.3 µm.

2.2. Galling tests and characterization

To simulate tribological conditions representative of hot metal forming processes with high degree of plastic deformation such as forging, wire drawing, and extrusion, testing was conducted using a high-temperature load-scanning tribometer (Fig. 4). Load-scanner employs a cross-cylinder contact geometry, in which the normal load progressively increases along the sliding path. This configuration enables each contact point to experience a unique load without prior loading history, thus generating a continuous profile of the coefficient of friction (COF) as a function of load. Such an approach facilitates the identification of critical loads associated with galling initiation and transfer layer build-up. A significant advantage of the load-scanner setup lies in its single-pass configuration, which ensures a continuous sliding contact with fresh sample surface. This makes it more representative of real forming conditions compared to conventional reciprocating sliding or pin-on-disc tribometers [26].

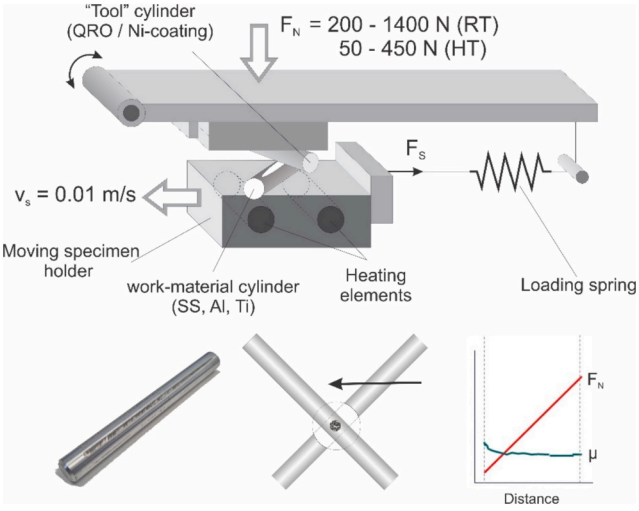

Fig. 4. Load-scanner configuration.

Tribological testing was carried out at room (RT) as well as elevated temperatures of 150 °C (SS) and 300 °C (Al, Ti), selected based on the typical temperatures used for warm and hot forming of the tested alloys, respectively. The lower moving specimen, representing the workpiece material, was heated by resistance heaters installed in the lower specimen holder and was sliding against upper stationary cylinder representing the tool/laser deposited coating. The sliding speed was fixed at 0.01 m/s, and the applied load was linearly increased along the 85 mm stroke length. For room temperature tests load was increased from 200 N to 1400 N and for elevated temperatures from 50 N to 450 N, in both cases resulting in significant plastic deformation of the counter-body cylinder. Different loads were selected for room and elevated temperature tests in order to initiate galling but prevent severe material transfer and transfer layer build-up, which could limit proper comparison and contact surface analysis. Although the testing was aimed at investigating the potential of Ni-based self-lubricating coatings for dry hot forming conditions, preliminary tests indicated the necessity for an additional solid lubricant to ensure stable operation. Therefore, a commercial graphite-based high temperature lubricant, commercially denoted as Bonderite© L-GP Aquadag (Henkel) was mixed with water and used as a baseline. The lubricant was prepared in a 15:85 vol. ratio with demineralized water, spread four times over the contact surface of the QRO 90 or laser cladded samples preheated to 130 °C, and left to dry prior to testing. Resulting solid lubricant layer thickness was ~15 μm.

Three parallel tests were carried out for each material combination and testing conditions, each one performed on a separate cylinder to account for any potential inhomogeneity of the laser deposition process. Single- and multi-cycle tests for up to 24 cycles were included in the investigation. The results were assessed by evaluating the coefficient of friction (COF) vs. load response, critical loads for galling initiation and transfer layer build-up, the volume of adhered counter-body material (Alicona G4 InfiniteFocus microscope), and detailed wear track characterization using SEM, EDS, and XPS. SEM/EDS analysis was performed by ZEISS Crossbeam 550 FIB-SEM Gemini II microscope and XPS by XPS Microprobe Versa Probe III (PHI).

3. Results and discussion

3.1. Preliminary dry tests

Preliminary high temperature dry sliding tests against AA6082 alloy (@300 °C) were aimed at identifying self-lubricating potential of Ni-5Ag-10MoS_2 laser coatings and possibility of additional solid lubricant elimination. Results are shown in Fig. 5. In the case of reference hot work tool steel (HWTS-QRO) galling has been initiated at the very beginning of the test, as indicated by high coefficient of friction of over 0.7. Similar conditions with the coefficient of friction being at the level of 0.65 are maintained up to the load of about 180 N. Between 200 N and 300 N we have a period of transfer layer formation and removal with very unstable friction, followed by gradual increase in friction due to transfer layer build-up. On the other hand, for Ni-5Ag-10MoS_2 coating initial coefficient of friction was below 0.3, but quickly galling has been initiated and increased coefficient of friction to about 0.45. This level has been maintained to about 150 N load, where more severe galling with transfer layer build-up caused jump in friction and its steady increase with load. Although for dry sliding conditions the investigated laser-deposited coatings incorporating Ag and MoS_2 provide about 30% lower friction as compared to reference HWTS-QRO, it is limited to low loads, below 200 N, but still being too high (> 0.4) with severe galling taking place at high loads, as shown in Fig. 5. This clearly indicates, that dry high-temperature forming between 150 °C and 300 °C is not feasible with 5Ag-10MoS_2 type of Ni-based coatings. Therefore, all further tests were performed combining application of water diluted graphite-based solid lubricant on the contact surface (15 μm; 15%) and looking at the potential improvement in friction control and galling reduction provided by the Ni-5Ag-10MoS_2 laser metal deposited coating.

Application of solid lubricant effectively reduces friction at elevated temperatures with its concentration and layer thickness playing an important role. For the concentration of 15% and layer thickness of 15 μm average coefficient of friction has been reduced to about 0.25, with the fluctuation of ±0.05 within the investigated load range (50–450 N). However, as shown in Fig. 6, reducing solid lubricant layer thickness below 5 μm resulted in the appearance of pronounced friction spikes (μ ≥ 0.4) and unstable friction, especially at low loads (< 200N), indicating solid lubricant film breakdown and galling initiation. Furthermore, reducing solid lubricant concentration from 15% to 7% further eliminated its friction and galling reducing potential, increasing coefficient of friction to about 0.5 and making it very unstable. Drop in friction at high loads is related to very high degree of Al-cylinder plastic deformation and reduced contact pressure.

3.2. Sliding against AA6082 alloy

Results for single sliding stroke galling test against AA6082 alloy performed at room and elevated temperature of 300 °C are shown in Figs. 7 and 8, respectively. Results are presented in the form of representative friction vs. load behavior (Figs. 7a and 8a), average coefficient of friction in low, medium and high loading regime (Figs. 7b), critical loads for galling initiation and transfer layer build-up (Figs. 7c), and volume of adhered AA6082 alloy material at low, medium and high loads (Figs. 7d and 8b). Identification of critical loads for galling initiation and transfer layer build-up (inserts in Fig. 7c) was based on the coefficient of friction instability (appearance of the first friction spikes)

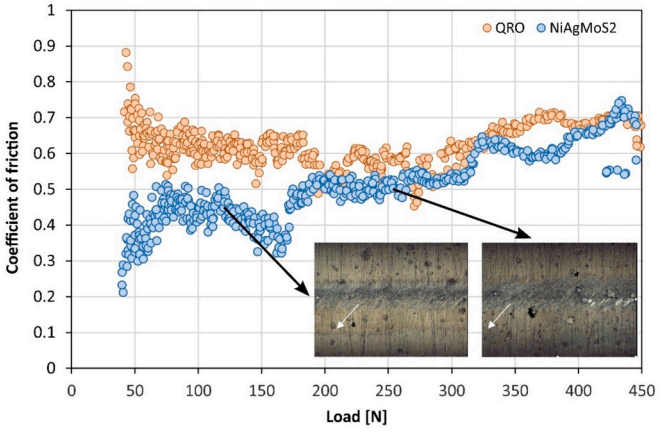

Fig. 5. Representative friction vs. load response for dry sliding galling tests against AA6082 alloy at 300 °C (white arrows indicate sliding direction).

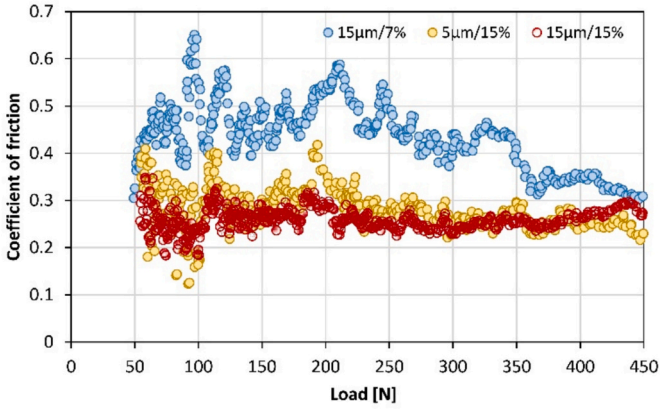

Fig. 6. Effect of solid lubricant concentration and layer thickness on friction behavior at 300 °C (Ni- coating - AA6082 sliding contact).

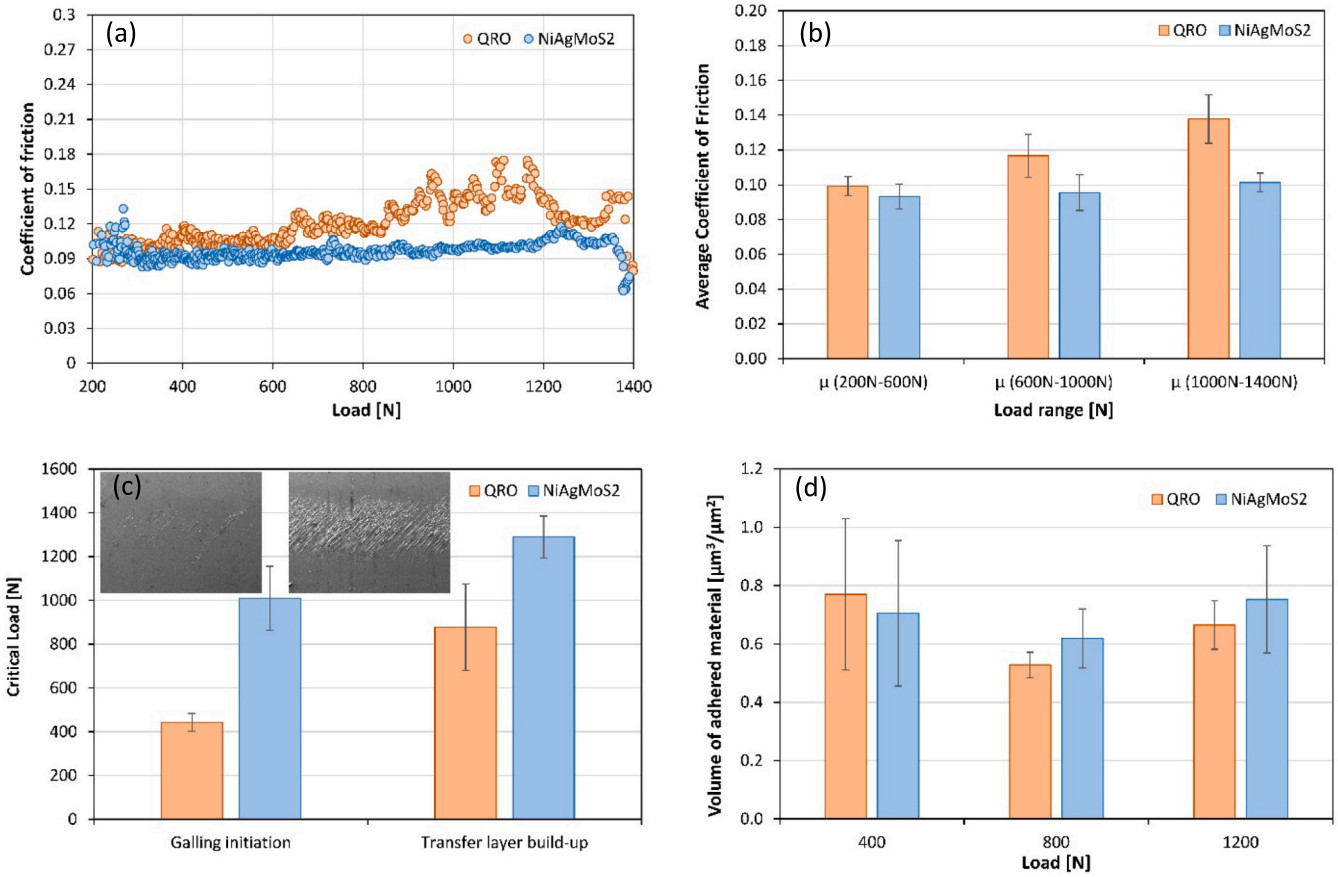

Fig. 7. Results of room temperature galling tests against AA6082 alloy; (a) CoF as a function of load, (b) average CoF in low, medium and high load range, (c) critical loads for galling initiation and transfer layer build-up, and (d) amount of adhered AA6082 alloy (volume per μm^2).

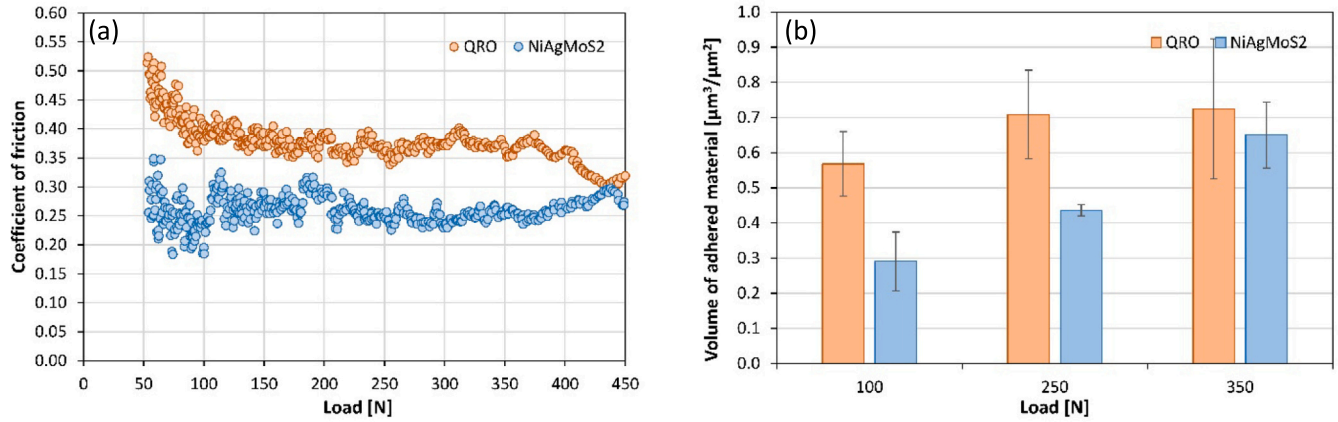

Fig. 8. Results of 300 °C galling tests against AA6082 alloy; (a) CoF as a function of load and (b) amount of adhered AA6082 alloy.

and wear track analyses (location of work material adhesion along the wear track), and is described in detail in Ref. [26].

In the case of room temperature tests first signs of unstable friction indicating galling initiation for HWTS-QRO were observed at load of about 440 N and transfer layer of AA6082 alloy build-up with very unstable friction at about 880 N. Ni-5Ag-10MoS_2 coating provided much more stable friction and less dependent on load, about 20% lower coefficient of friction as compared to HWTS-QRO, especially at high loads and more than 50% better galling resistance, as shown in Fig. 7. On the other hand, for both tool materials (HWTS-QRO and Ni-5Ag-10MoS_2) similar level of AA6082 alloy adhesion on the sliding wear track was detected, without very specific load dependency (Fig. 7d). Also at high temperature tests (300 °C) Ni-5Ag-10MoS_2 coating provided lower friction (~30%) and better galling resistance, with higher critical loads for galling initiation and up to 50% reduced volume of adhered AA6082 alloy, as shown in Fig. 8.

When performing multicycle galling tests (25 cycles for room temperature conditions and 15 cycles for high temperature conditions),

beneficial effect of Ni-5Ag-10MoS_2 coating is displayed in the form of more stable friction maintained in wider load range and for higher number of cycles, as shown by 3D friction maps displayed in Fig. 9. In the case of room temperature multicycle tests against AA6082 alloy, Ni-5Ag-10MoS_2 coating provided low and stable friction throughout the whole investigated load range (200−1100N) for 10–15 cycles. On the other hand, for HWTS-QRO, with higher friction and galling tendency, unstable friction behavior took place already after 2–3 cycles (Fig. 9a and b). At elevated temperature of 300 °C difference in friction behavior between HWTS-QRO and Ni-5Ag-10MoS_2 coating is very minor and limited to high loads (Fig. 9c and d), but as for single stroke test coating provided considerably higher galling resistance in terms of adhered AA6082 alloy, as shown in Fig. 10b.

3.3. Sliding against AISI 316L stainless steel

Also in the case of galling tests against AISI 316L (1.4404) stainless steel, Ni-5Ag-10MoS_2 coating provides improved tribological performance. However, better anti-galling performance is mainly related to room temperature conditions. In contrast to Al-alloy, austenitic stainless steel undergoes strain-induced martensitic transformation during plastic deformation [27] thus showing more pronounced hardness increase and putting higher stress on the solid lubricant film during testing. Consequently, higher and more unstable friction with reduced critical galling loads are observed for HWTS-QRO against AISI 316L stainless steel, as shown in Fig. 11a, b and c. Reduced volume of adhered material (Fig. 11d) can also be related to higher work-hardening effect in stainless steels and thus reduced galling tendency as compared to Al-alloys. However, with rapid solid lubricant film break-down self-lubricating performance of Ni-5Ag-10MoS_2 coating against AISI 316L stainless steel becomes more pronounced. As shown in Fig. 11, at room temperature Ni-5Ag-10MoS_2 coating gave much more stable and over 50% lower coefficient of friction than HWTS-QRO tool steel, about 30% higher critical loads for galling initiation and transfer layer build-up, and 50–60% reduction in volume of adhered AISI 316L stainless steel on the contact surface. On the other hand, for elevated temperature galling tests performed at 150 °C (warm stainless steel forming) both materials showed low coefficient of friction (~0.1) with similar friction behavior, and no difference in critical loads. This can be related to increased lubricity of MoS_2 solid lubricant film at 150 °C [6], thus masking positive effect of Ni-5Ag-10MoS_2 coating. Anyway, Ni-5Ag-MoS_2 coating still provided 20–30% better galling resistance in terms of volume of adhered workpiece material, which intensifies with applied load, as shown in Fig. 12.

Under multicycle testing mode differences between HWTS-QRO and Ni-5Ag-10MoS_2 are more pronounced, as displayed in Fig. 13. In the case of room temperature tests with HWTS-QRO coefficient of friction increased to values well over 0.5 in just 2 cycles for the whole load range investigated (low to high). Ni-5Ag-10MoS_2 coating on the other hand, provided long-term low and stable friction in the low load regime, while in medium and high load regime low friction can be maintained for 5–10 cycles (Fig. 13b), which also resulted in substantially reduced volume of adhered material (Fig. 14a). When switching to high temperature testing (150 °C), difference between HWTS-QRO and Ni-5Ag-10MoS_2 is harder to distinguish, with both showing similar friction behavior in low load range. However, Ni-5Ag-10MoS_2 coating still resulted in about 20% lower and slower increasing friction at medium and high loads, and reduced AISI 316L stainless steel adhesion, as shown in Fig. 14a and b.

3.4. Sliding against Ti6Al4V alloy

In the case of Ti6Al4V alloy application of Ni-5Ag-10MoS_2 coating resulted in similar or even slightly higher coefficient of friction, as compared to HWTS-QRO (Fig. 15a and b). Ti6Al4V alloy is known as the material being notoriously susceptible to galling [28], thus showing the

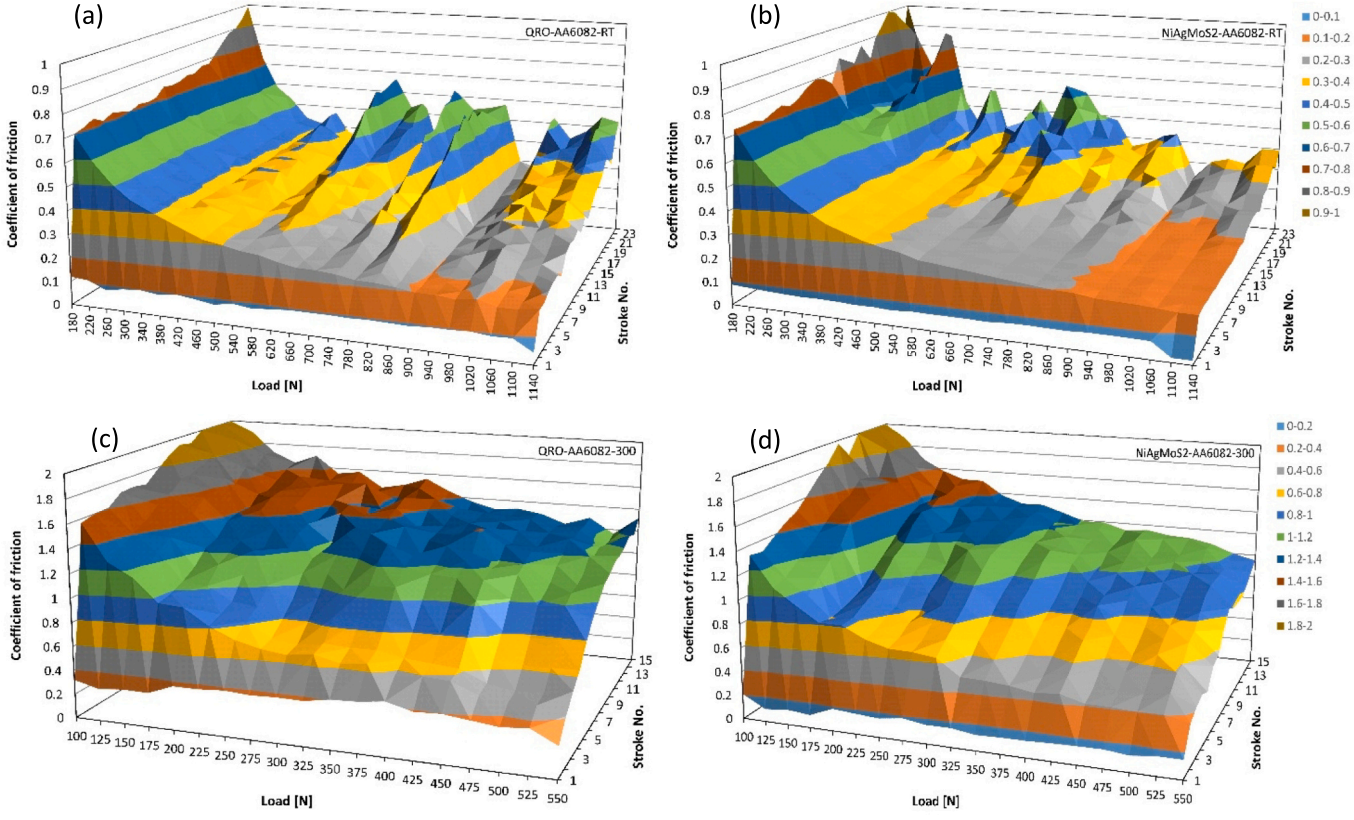

Fig. 9. 3D friction maps for (a and b) room and (c and d) elevated temperature multicycle galling test against AA6082 alloy.

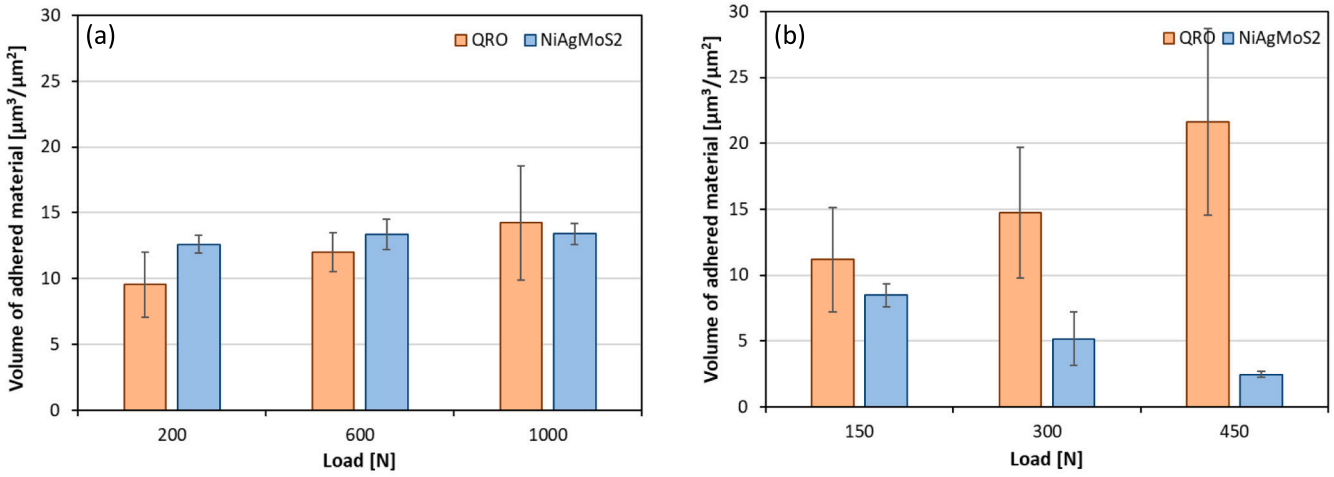

Fig. 10. Volume of adhered AA6082 alloy for multicycle galling tests at (a) room temperature and (b) 300 °C.

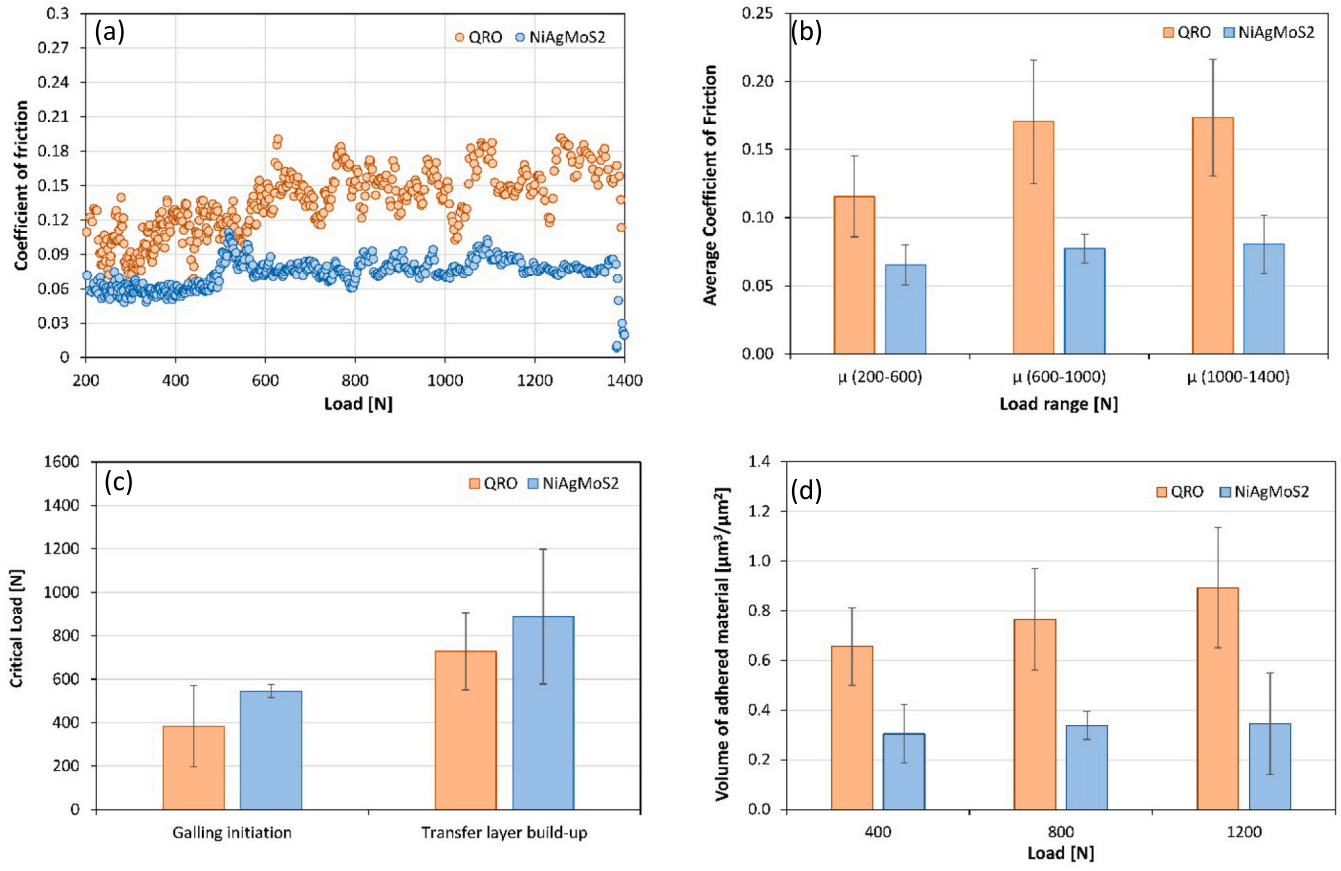

Fig. 11. Results of room temperature galling tests against AISI 316L stainless steel; (a) CoF as a function of load, (b) average CoF in low, medium and high load range, (c) critical loads for galling initiation and transfer layer build-up, and (c) amount of adhered stainless steel.

highest friction among the alloys tested and immediate galling initiation with a thick transfer layer build-up. However, despite rapid and intense galling of the Ti6Al4V alloy on both tool materials (see Section 3.5), Ni-5Ag-10MoS_2 coating still indicates better galling resistance against Ti-alloy, as displayed by more stable friction and reduced thickness/volume of adhered material (Fig. 15c and d). Also under repeated sliding cycles both tool materials showed almost identical friction response, being determined by immediate formation of thick transfer layer. However, Ni-5Ag-10MoS_2 is still superior in terms of volume of adhered Ti-alloy, as shown in Figs. 16 and 17.

3.5. *Wear track analysis*

SEM/EDS-mapping analysis of wear track for Ni-5Ag-10MoS_2 – AA6082 contact at room temperature and mid-load range (800 N) is shown in Fig. 18. The graphite-based solid lubricant with its layered structure and easy sharing characteristics [29] applied on the contact surface of HWTS-QRO or Ni-5Ag-10MoS_2 cylinder before the test

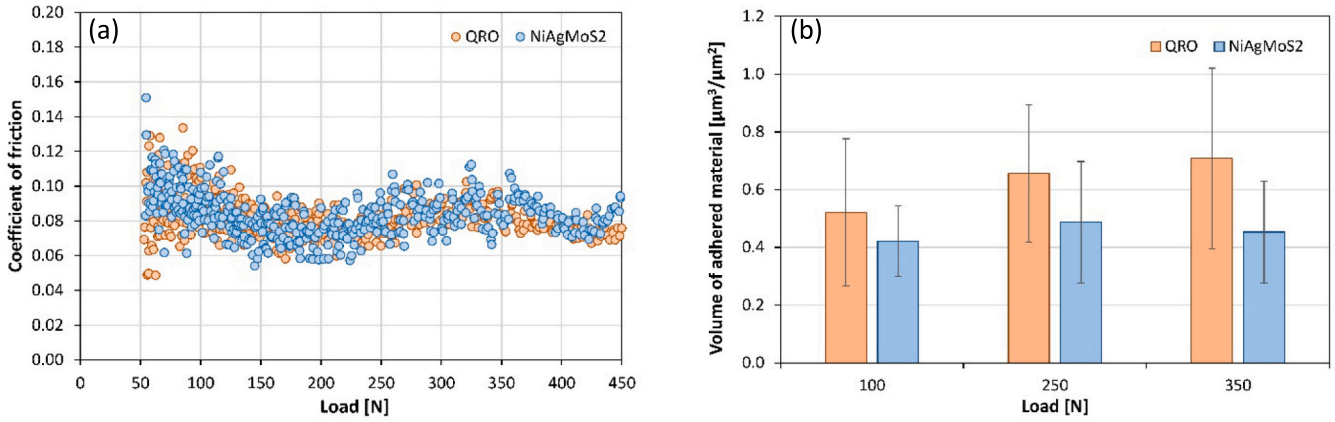

Fig. 12. Results of 150 °C galling tests against AISI 316L stainless steel; (a) CoF as a function of load and (b) amount of adhered stainless steel.

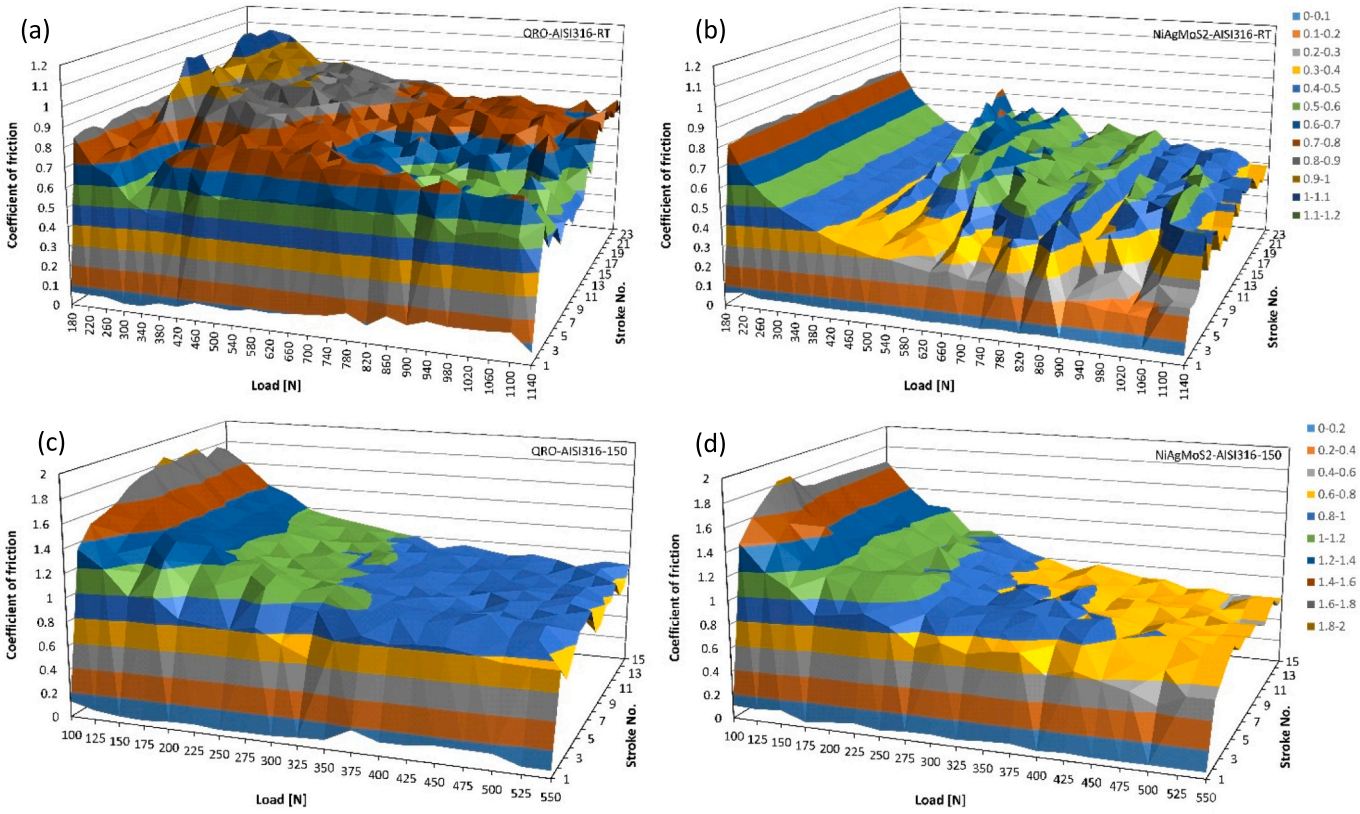

Fig. 13. 3D friction maps for (a and b) room and (c and d) elevated temperature multicycle galling test against AISI 316L stainless steel.

provided certain degree of protection against adhesion of AA6082 alloy and galling. However, this protection is limited to room temperature and low loads (< 400 N) as indicated by increase and instability of the coefficient of friction (Figs. 7a–b and 8a–b), and wear track analysis. At higher loads strength of the MoS_2 layer is exceeded leading to its removal and localized adhesion of the Al-alloy on the contact surface. Although surface topography analysis did not reveal any significant difference in roughness increase after the galling test between reference tool steel and Ni-5Ag-10MoS_2 coating, certain differences were identified by wear track microscopy, as indicated in Fig. 19. In the case of Ni-5Ag-10MoS_2 coating patches of integrated Ag-MoS_2 solid lubricant locally prevented Al-alloy adhesion (Fig. 19d), which resulted in more stable friction (Fig. 7a), higher critical loads (Fig. 7c) and postponed galling with thin (<0.5 µm) and quite evenly distributed areas of Al-transfer layer around the Ag-MoS_2 patches (Figs. 18, and 19c and d). On the other hand, for HWTS-QRO thicker (> 1 µm), more concentrated and larger, but unevenly distributed areas of adhered Al-alloy were observed, with the difference in size and distribution of adhered Al-alloy escalating at elevated temperatures, as shown in Fig. 19.

At room temperature adhesion of Al-alloy is mainly controlled by contact pressure and due to large plastic deformation of the Al-cylinder taking place already at low loads (< 400 N) similar volume of adhered Al-alloy material over the contact surface was detected for a broad load range (400–1200 N) and both tool materials investigated, as shown in Fig. 7d. However, in the case of HWTS-QRO we have thicker and more unevenly distributed areas of adhered Al-alloy, thus resulting in higher

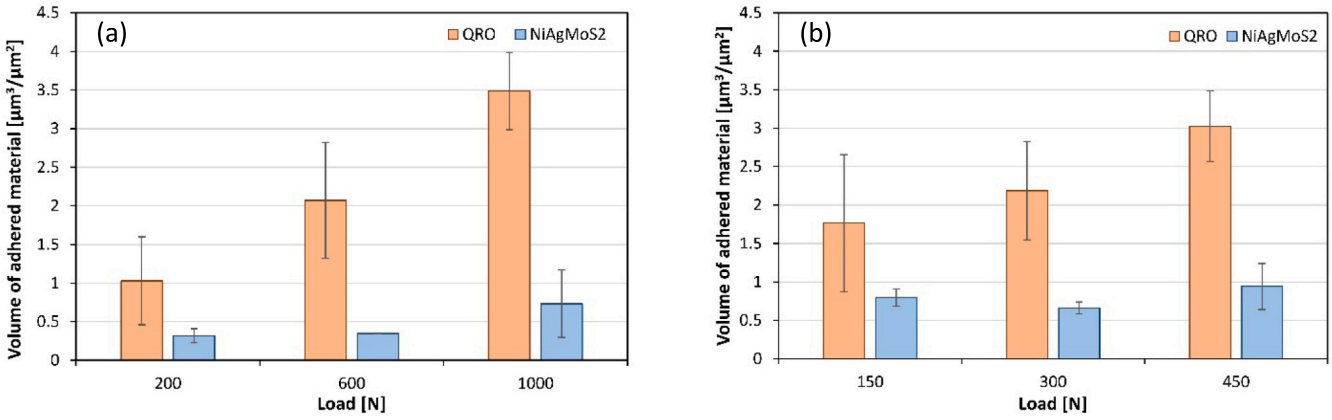

Fig. 14. Volume of adhered AISI 316L stainless steel for multicycle galling tests at (a) room temperature and (b) 150 °C.

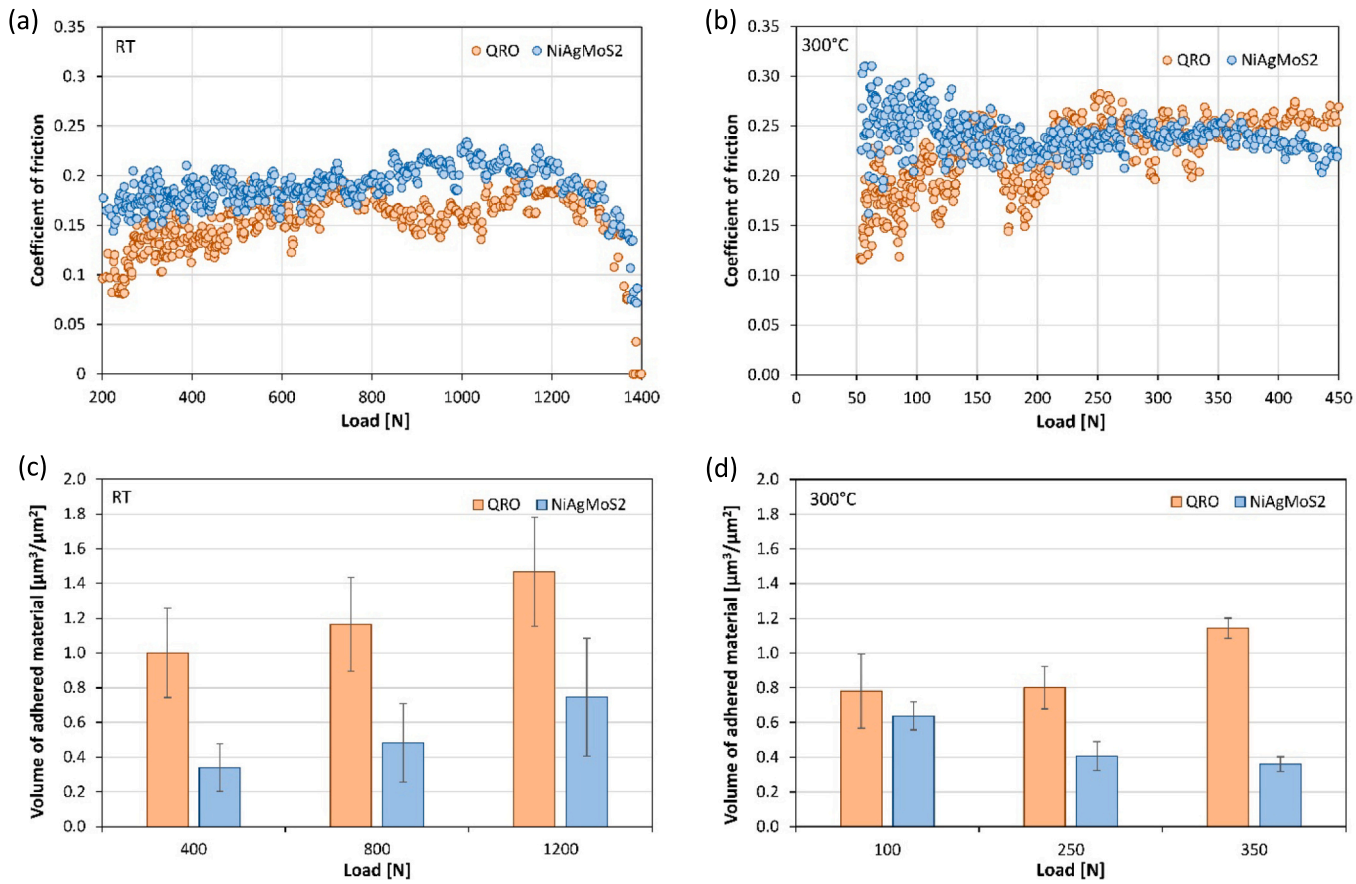

Fig. 15. Results of (a and c) room and (b and d) elevated temperature (300 °C) single-stroke galling tests against Ti6Al4V alloy; (a and b) CoF as a function of load and (c and d) amount of adhered Ti6Al4V alloy.

and more unstable friction (Fig. 7a and b) as well as faster galling advancement under repeated sliding (Fig. 9a and b). Increased reactivity and plasticity of the Al-alloy at elevated temperatures [30] resulted in higher friction, intensified galling and more pronounced differences between HWTS-QRO and Ni-5Ag-10MoS_2 coating.

Better galling resistance of Ni-5Ag-10MoS_2 coating at room temperature is mainly provided by Cr_2S_3/Cr_3S_4 [14], as identified by FIB-SEM (Fig. 20) and XPS analysis (Fig. 21) of the wear track where adhesion of the Al-alloy was prevented. After surface cleaning XPS analysis didn't reveal any MoS_2, with the Mo $3d_{5/2}$ peak positioned at 228.1 eV (Fig. 21a), indicating Mo-carbide. Also for Ag only signal for metallic Ag, positioned at 368.4 eV was identified (Fig. 21c). Although Cr XPS signal (Fig. 21b) was too weak for detailed analysis, overlapping of Cr and S EDS signals (Figs. 18 and 20) and the S 2p core sulfide peak at 162.8 eV [31] (Fig. 21d) confirm MoS_2 decomposition during laser metal deposition of the coating and formation of Cr_3S_4 [14]. At elevated temperatures Ag located at the contact surface provided additional protection against galling by its low shear strength [32] and formation of Ag_2S. It is formed through interaction of sulfide-rich phases and Ag at the sliding interface [33]. No Ag-molybdate could be identified while

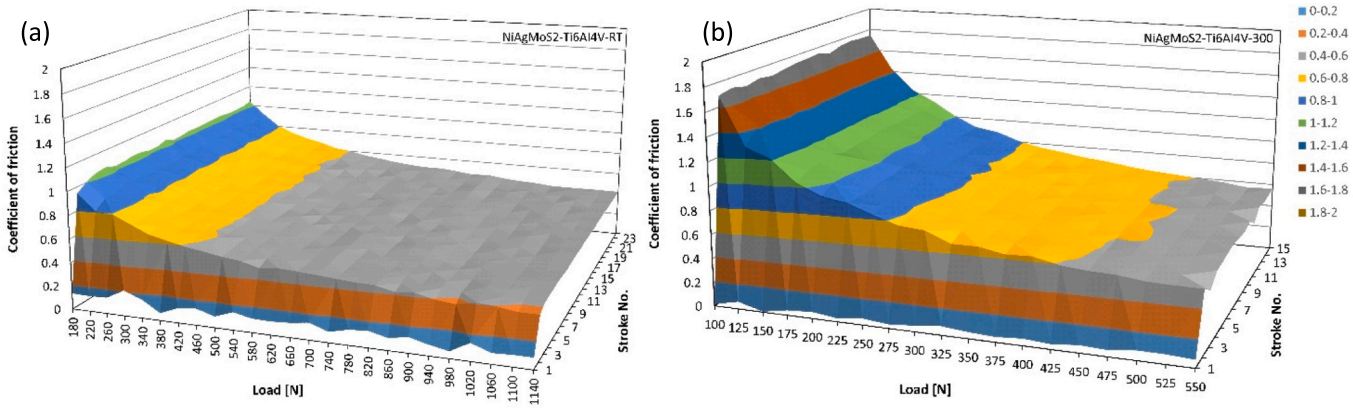

Fig. 16. 3D friction maps for (a) room and (b) elevated temperature multicycle galling test of Ni-5Ag-10MoS2 coating against Ti6Al4V alloy.

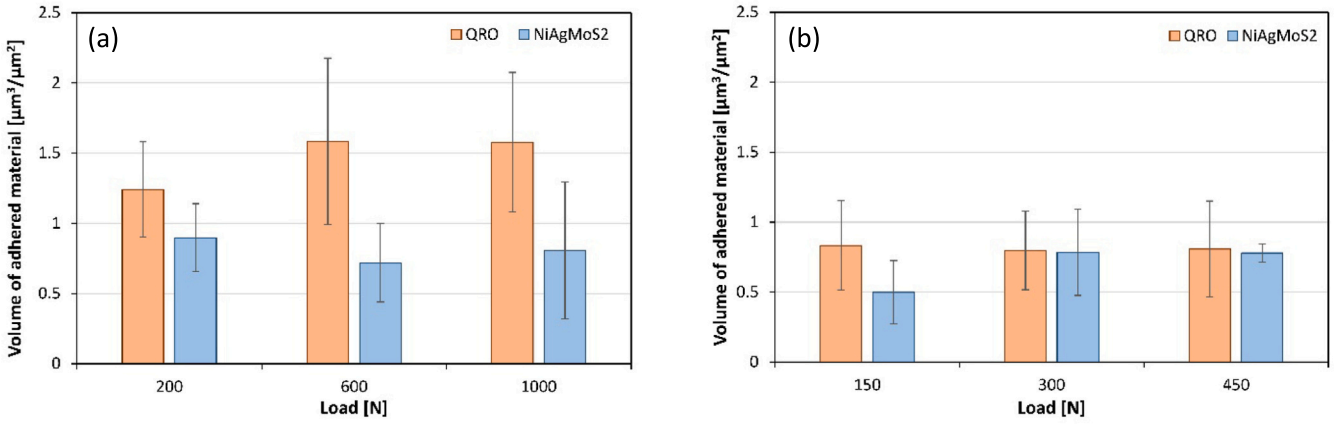

Fig. 17. Volume of adhered Ti6Al4V alloy for multicycle galling tests at (a) room temperature and (b) 300 °C.

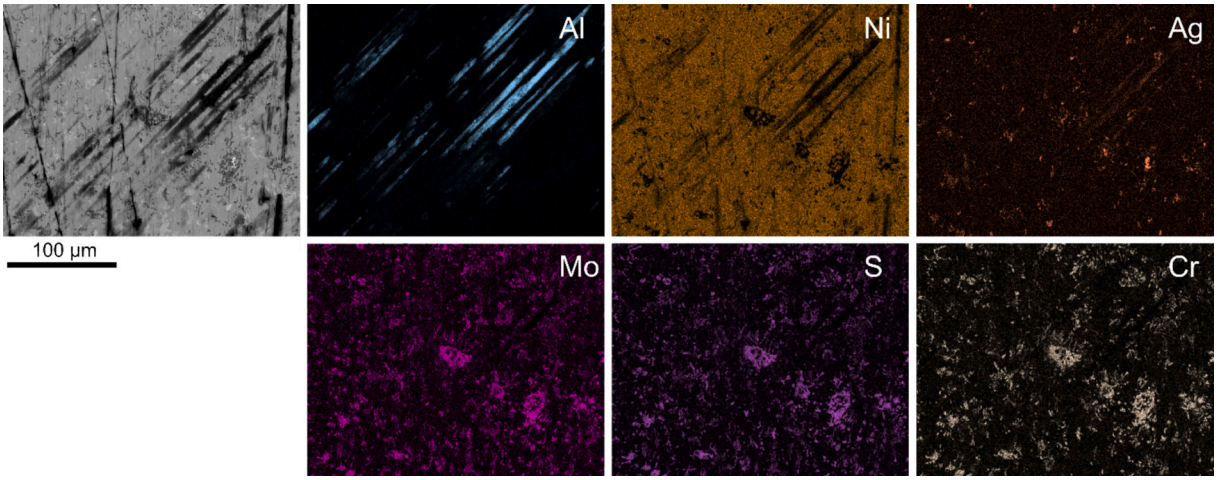

Fig. 18. (a) SEM wear track micrograph and (b) corresponding EDS maps for Ni-5Ag-10MoS$_2$ – AA6082 contact (room temperature, 800 N); Mo and S signals overlap.

binding energies of the Ag $3d_{5/2}$ and $3d_{3/2}$ spin-orbit pair positioned at 367.7 eV and 373.6 eV (Fig. 21c) and the S $2p_{3/2}$ peak at 161.3 eV (Fig. 21d) are indicative of Ag_2S formation [34]. Furthermore, beside Ag_2S and Cr_2S_3/Cr_3S_4 also Cr_2O_3 was identified for high temperature tests (Cr 2p3/2 peak components at 574.5 eV (sulfide) and 576 eV (oxide), Fig. 21b), which can also provide some beneficial high-temperature tribological properties [35]. Combination of these low friction compounds very effectively postponed Al-alloy adhesion, as shown in Fig. 19d. It also reduced bonding strength of the adhered Al-patches, which could be more effectively removed under repeated sliding and high loads, as indicated by reduced volume of adhered material displayed in Fig. 10b.

Very similar situation was observed for tests against AISI 316L stainless steel, with incorporated islands of Cr_2S_3/Cr_3S_4 effectively

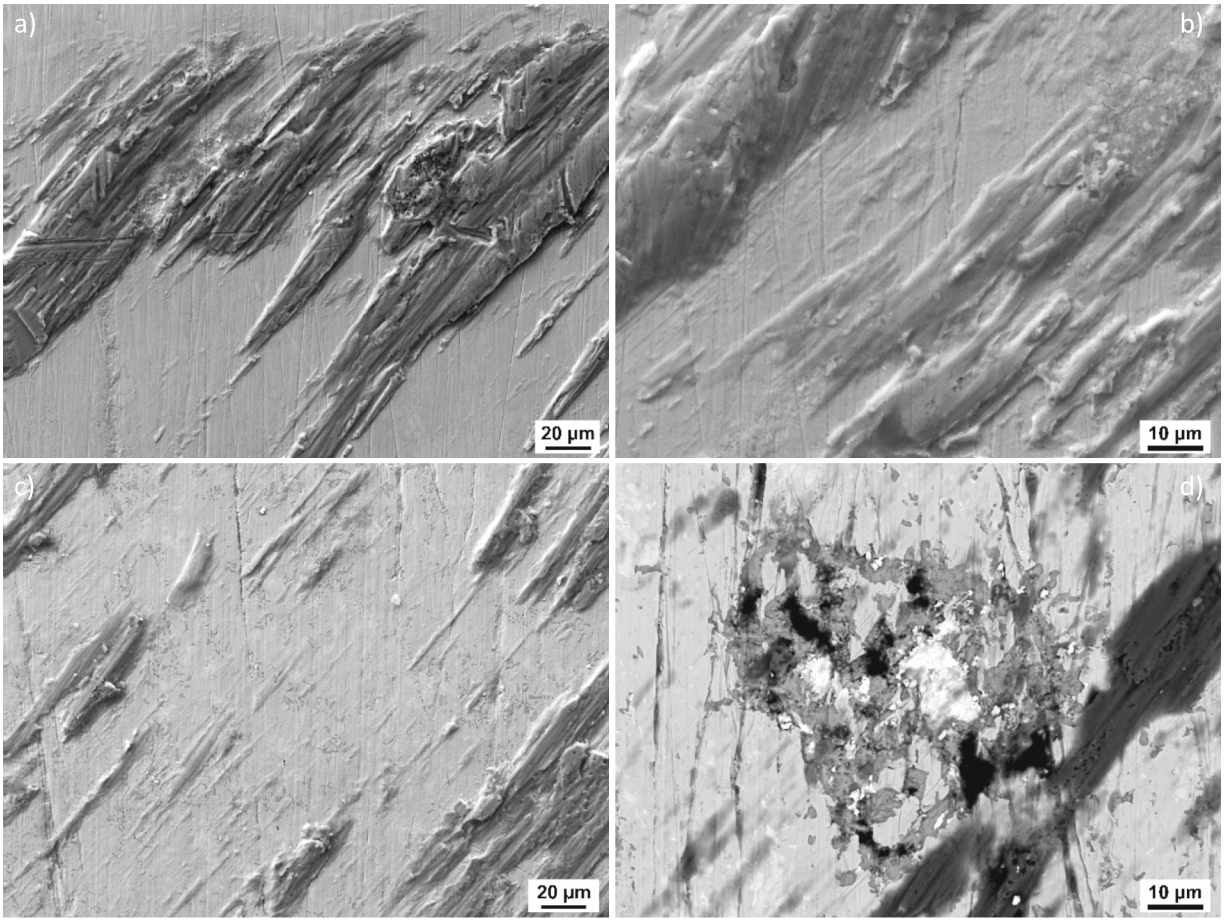

Fig. 19. Wear track micrographs for high temperature contact (250 N); (a and b; SE image) HWTS-QRO - AA6082, (c-SE and d-BSE image) Ni-5Ag-10MoS_2 – AA6082 contact.

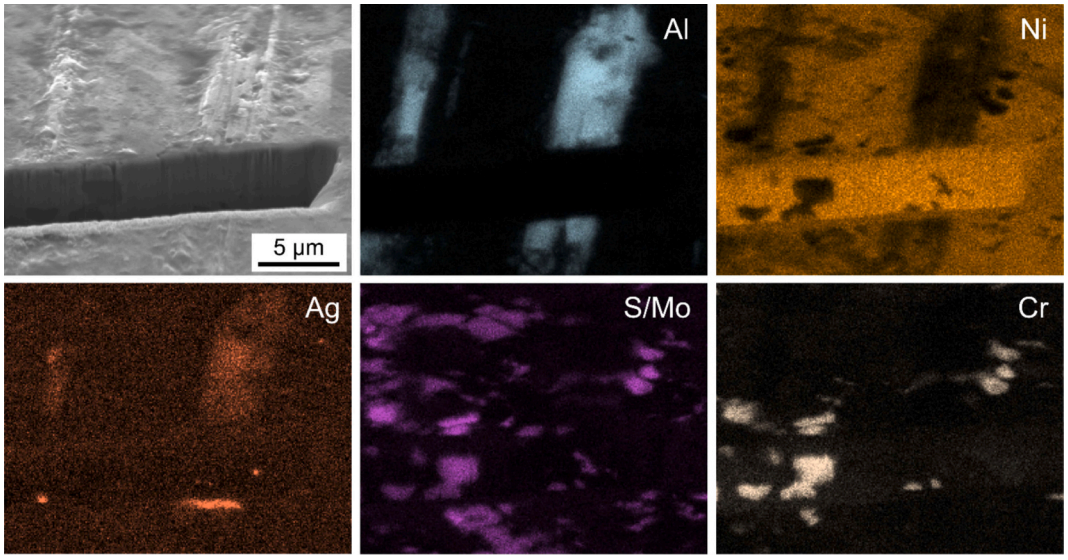

Fig. 20. FIB-SEM analysis of Ni-5Ag-10MoS_2 wear track (room temperature, 800 N).

preventing/postponing stainless steel adhesion and accumulation on the coating surface, as shown in Fig. 22. However, as already mentioned, more pronounced AISI 316L austenitic stainless steel work-hardening behavior reduced the protective effect of applied MoS_2 solid lubricant, thus intensifying anti-galling performance of Ni-5Ag-10MoS_2 coating (Fig. 11) as compared to AA6082 alloy (Fig. 7). At elevated temperature of 150 °C, which was too low for Ag_2S formation [36,37], improved lubricity of MoS_2 combined with reduced shear strength of the stainless steel resulted in much smaller and more evenly distributed patches of adhered stainless steel, even for HWTS-QRO (Fig. 22c and f). Although

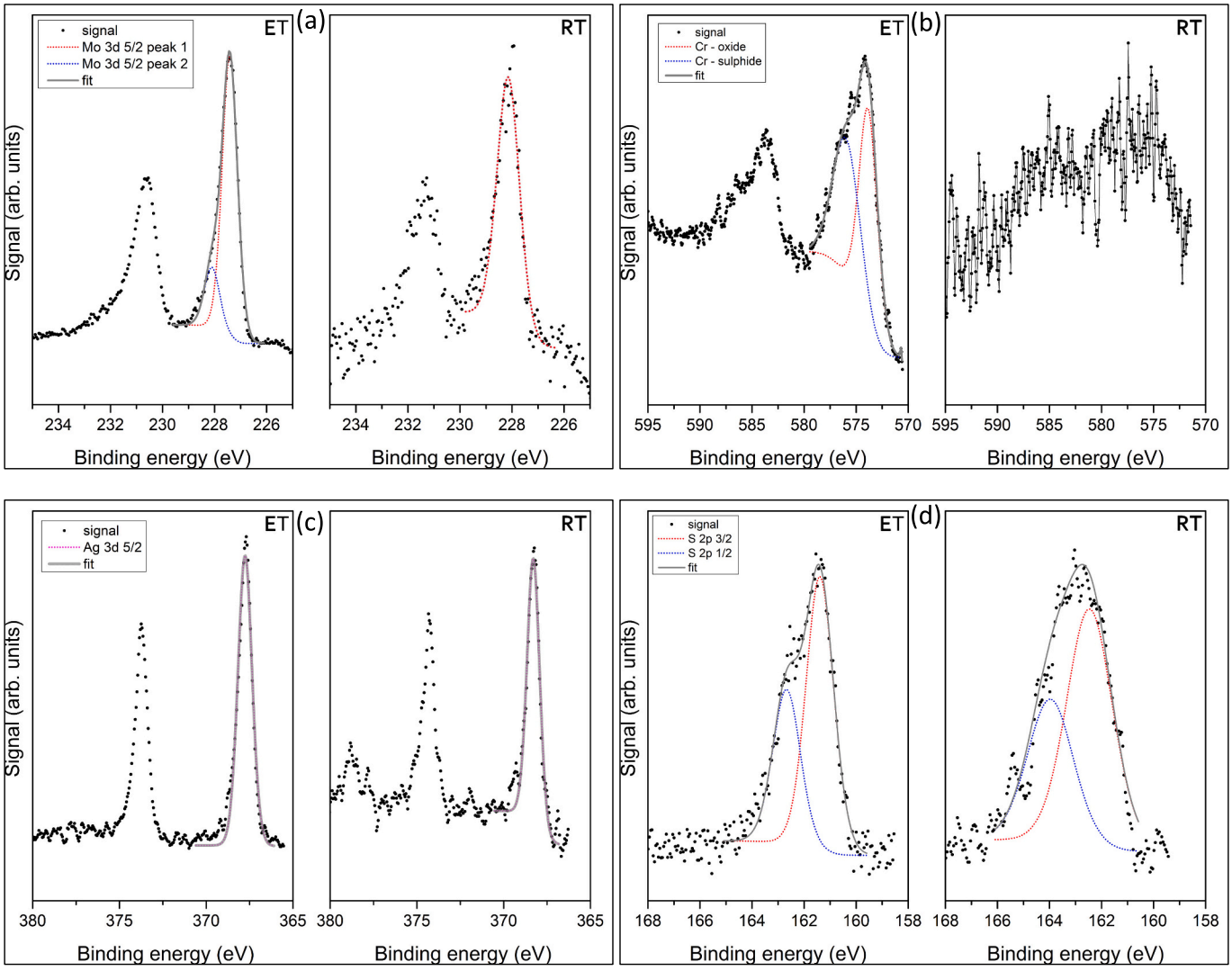

Fig. 21. XPS spectra from contact surface of Ni-5Ag-10MoS_2 coating tested at room (RT) and elevated temperature (ET); (a) Mo 3d, (b) Cr 2p, (c) Ag 3d, (d) S 2p.

Ni-5Ag-10MoS_2 coating reduces stainless steel adhesion, smaller and more evenly distributed patches of adhered stainless steel control the overall friction level, irrespective of the tool material used, as exemplified by Fig. 12a.

For Ti6Al4V alloy, being very prone to galling, severe adhesion and formation of thick transfer layer took place for both tool materials already at room temperature and very low loads, as shown in Fig. 23. In this case shear strength of the Ti6Al4V transfer layer defines friction level, thus leading to very similar friction behavior for reference hot work tool steel and Ni-5Ag-10MoS_2 coating (Figs. 15a and b). And this is true for room and elevated temperature sliding. However, as indicated by BEI images (Fig. 23d), in the case of Ni-5Ag-10MoS_2 coating layer of adhered Ti-alloy is more easily interrupted and displaced at the Ag-Cr_2S_3/Cr_3S_4 islands, resulting in a thinner transfer layer (Fig. 15c). This is further pronounced at elevated temperatures (Fig. 15d) by the formation of Ag_2S. Under repeated multicycle sliding immediate formation of a thick transfer layer during the very first stroke greatly masks effectiveness of the lubricating phases, especially at elevated temperature with increased Ti-alloy galling tendency. However, presence of lubricious phases in Ni-5Ag-10MoS_2 coating still promotes easier detachment of transfer layer during repeated sliding and reduced redeposition (Fig. 17).

Anti-galling mechanism of Ni-5Ag-10MoS_2 coating is illustrated in Fig. 24. In the case of tool steel increased loads and plastic deformation of the work material lead to rapid MoS_2 lubrication film break-down and intensive adhesion of work material to the tool surface. Sliding at gradually increasing load results in the formation of thick, largely interconnected patches of transfer layer (Fig. 24a), which intensifies with increased temperature and work material galling tendency (SS → Al → Ti). For Ni-5Ag-10MoS_2 coating encapsulated solid-lubrication compounds with their low shear strength postpone adhesion of work material and provide formation of much thinner and largely scattered patches of transfer layer. Furthermore, smearing of the lubricious compounds over the contact surface and formation of a tribolayer also reduces bonding strength of these patches, which are more easily detached during sliding (Fig. 24b). In the case of sliding at temperatures of up to 150 °C improved galling resistance is mainly provided by Cr-sulfides (CrS, Cr_2S_3/Cr_3S_4) formed during coating deposition. However, at elevated temperature of 300 °C, main anti-galling component is silver, accompanied by Cr-sulfides and formation of Ag_2S and Cr_2O_3.

4. Conclusions

The present study demonstrates that Ni-5Ag-10MoS_2 laser metal deposited coatings with temperature resistant load-bearing Ni-based matrix can provide substantial improvements in galling resistance over conventional hot work tool steels, even for room and intermediate temperatures. Under both room and elevated temperature sliding

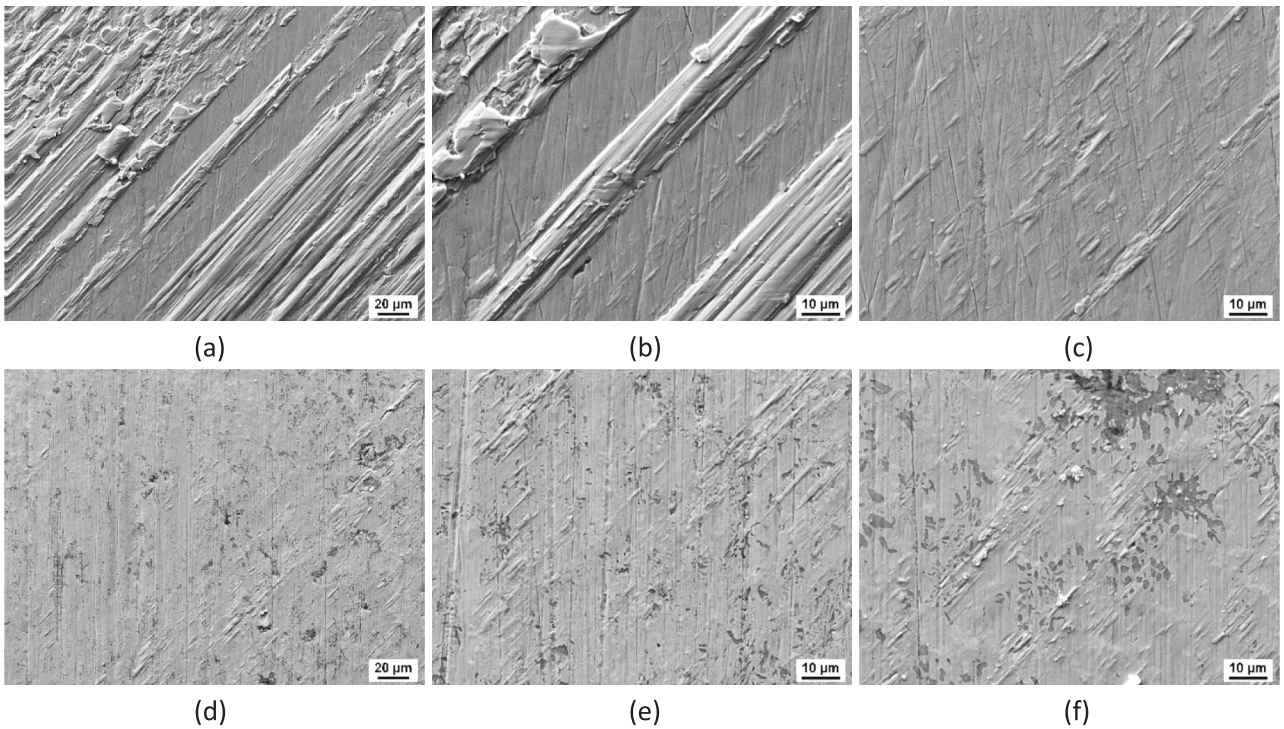

Fig. 22. SEM wear track micrographs for (a, b, d, e) room (800 N) and (c, f) high temperature contact (150 °C; 250 N); (a–c) HWTS-QRO – AISI316L and (d–f) Ni-5Ag-10MoS_2 – AISI316L contact.

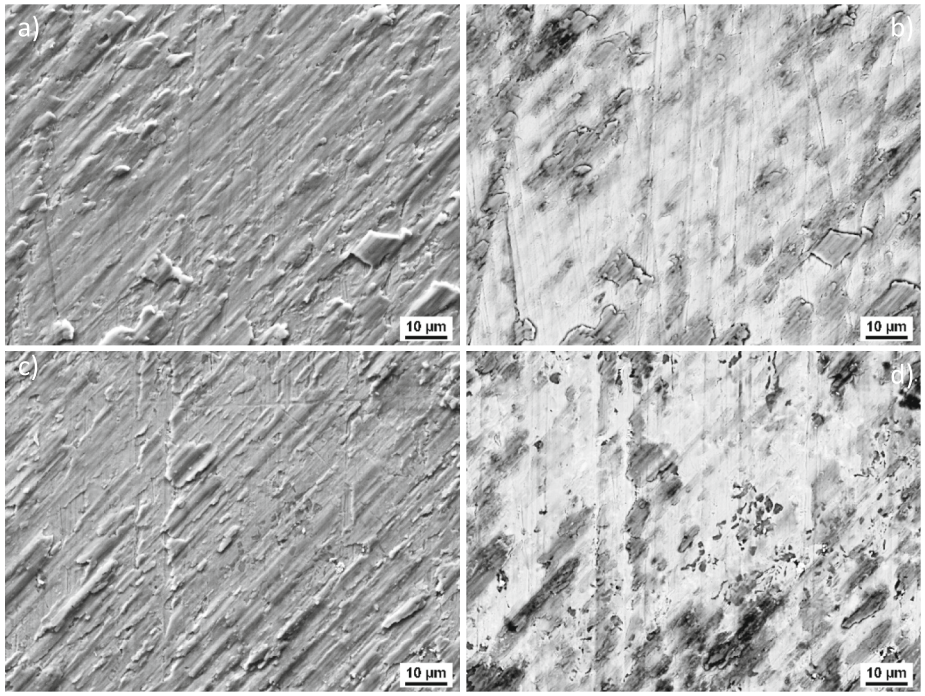

Fig. 23. SEM/BSE wear track micrographs for room temperature contact (400 N); (a, b) HWTS-QRO – Ti6Al4V and (c, d) Ni-5Ag-10MoS_2 – Ti6Al4V contact.

against AA6082 and AISI 316L alloys, the coatings reduce friction by up to 50%, provide about 30% higher critical loads for galling initiation, and suppress material adhesion. At room temperature counter-body material adhesion is suppressed by the Cr_2S_3/Cr_3S_4 compounds formed by the MoS_2 decomposition during laser metal deposition. However, at elevated temperatures anti-galling properties of Cr_2S_3/Cr_3S_4 are further enhanced through synergistic effect of in-situ formation of lubricious Ag_2S and/or Cr_2O_3 tribo-compounds at the interface. While galling against Ti6Al4V remains severe, the Ag-MoS_2 containing Ni-based coatings promote thinner, less continuous transfer layers, particularly at 300 °C. Multicycle testing further confirms that the coatings sustain stable low-friction conditions over extended operation and wider load ranges while reducing adhered material accumulation. These findings highlight the potential of Ni-Ag-MoS_2-based

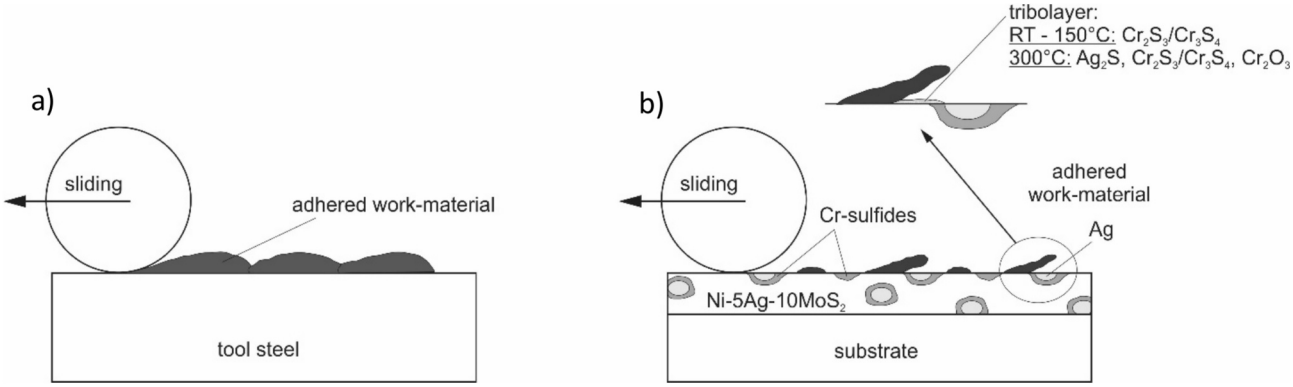

Fig. 24. Schematic of a galling mechanism for (a) tool steel and (b) Ni-5Ag-10MoS_2 laser deposited coating.

coatings as effective anti-galling solutions for high-temperature forming of high-strength structural alloys.

Particular Ni-based self-lubricating coating combined with MoS_2-based solid lubricant was found as the most effective against Al alloys at 300 °C. Al alloys have low work-hardening effect and increased galling tendency at elevated temperatures thus fully exploiting combined effect of solid lubricant and Cr/Ag lubricious phases formation. Austenitic stainless steels, on the other hand experience strain-induced martensitic transformation during cold forming which greatly limits effectiveness of solid lubricant and facilitates anti galling potential of the coating. However, in warm forming at 150 °C reduced martensitic transformation and absence of Ag_2S formation prevent any major performance improvement. In the case of Ti-alloys anti-galling potential of the coating is hindered by the severe galling and immediate formation of thick transfer layer, although the coating providing more effective removal of the adhered material.

CRediT authorship contribution statement

B. Podgornik: Writing – review & editing, Writing – original draft, Visualization, Supervision, Project administration, Formal analysis, Data curation. **V. Yarasu:** Investigation, Data curation. **B. Šetina Batič:** Formal analysis, Data curation. **M. Rodriguez Ripoll:** Writing – original draft, Project administration, Funding acquisition, Conceptualization.

Declaration of competing interest

The authors declare that they have no known competing financial interests or personal relationships that could have appeared to influence the work reported in this paper.

Acknowledgement

This work was funded by the Austrian Research Promotion Agency/ Österreichische Forschungs-förderungsgesellschaft (FFG) (Project K2 XTribology, Grant No. 849109) and has been carried out within the 'Austrian Excellence Center for Tribolog' (AC2T research GmbH) and Institute of Metals and Technology (IMT) with the financial support from the Slovenian Research and Innovation Agency (research core funding No. P2-0050). Authors would like to thank dr. Črtomir Donik for FIB-samples preparation and characterization.

Data availability

Link to my data is shared: https://doi.org/10.5281/zenodo.18015576

References

[1] K. Dohda, M. Yamamoto, C. Hu, L. Dubar, K.F. Ehmann, Galling phenomena in metal forming, Friction 9 (2021) 665–685.
[2] B. Podgornik, Adhesive wear failures, J. Fail. Anal. Prev. 22 (2022) 113–138, https://doi.org/10.1007/s11668-021-01322-4.
[3] R. Ganesh Narayanan, Jay S. Gunasekera, Sustainable Material Forming and Joining, CRC press, Boca Raton, 2019, https://doi.org/10.1201/9781315163147.
[4] K. Dohda, C. Boher, F. Rezai-Aria, et al., Tribology in metal forming at elevated temperatures, Friction 3 (2015) 1–27, https://doi.org/10.1007/s40544-015-0077-3.
[5] J.-H. Ouyang, Y.-F. Li, Y.-Z. Zhang, Y.-M. Wang, Y.-J. Wang, High-temperature solid lubricants and self-lubricating composites: a critical review, Lubricants 10 (2022) 177, https://doi.org/10.3390/lubricants10080177.
[6] R. Kumar, I. Hussainova, R. Rahmani, M. Antonov, Solid lubrication at high-temperatures—a review, Materials 15 (2022) 1695, https://doi.org/10.3390/ma15051695.
[7] B. Podgornik, T. Kosec, A. Kocijan, Č. Donik, Tribological behaviour and lubrication performance of hexagonal boron nitride (h-BN) as a replacement for graphite in aluminium forming, Tribol. Int. 81 (2015) 267–275, https://doi.org/10.1016/j.triboint.2014.09.011.
[8] P. Carlsson, M. Olsson, PVD coatings for sheet metal forming processes—a tribological evaluation, Surf. Coat. Technol. 200 (2006) 4654–4663, https://doi.org/10.1016/j.surfcoat.2004.10.127.
[9] B. Podgornik, J. Vižintin, S. Hogmark, Improvement in galling performance through surface engineering, Surf. Eng. 22 (2006) 235–238, https://doi.org/10.1179/174329406X122946.
[10] R. Franz, C. Mitterer, Vanadium containing self-adaptive low-friction hard coatings for high-temperature applications: a review, Surf. Coat. Technol. 228 (2013) 1–13.
[11] Wang Cuicui, Xu Beibei, Wang Zhenyu, Li Hao, Wang Li, Chen Rende, Wang Aiying, Ke Peiling, Tribological mechanism of (Cr, V)N coating in the temperature range of 500–900°C, Tribol. Int. 159 (2021) 106952.
[12] D.M. Walters, K.M. White, U. Patel, M.J. Davis, R.M. Veluci-Marlow, S. R. Bhupanapadu Sunkesula, et al., Genetic susceptibility to interstitial pulmonary fibrosis in mice induced by vanadium pentoxide (V2O5), FASEB J. 28 (2014) 1098–1112, https://doi.org/10.1096/fj.13-235044.
[13] M.M. Quazi, M.A. Fazal, A.S.M.A. Haseeb, et al., A review to the laser cladding of self-lubricating composite coatings, Lasers Manuf. Mater. Process. 3 (2016) 67–99, https://doi.org/10.1007/s40516-016-0025-8.
[14] H. Torres, T. Caykara, J. Hardell, J. Nurminen, B. Prakash, M. Rodríguez Ripoll, Tribological performance of iron- and nickel-base self-lubricating claddings containing metal sulfides at high temperature, Friction 10 (2022) 2069–2085, https://doi.org/10.1007/s40544-021-0578-1.
[15] Suiyuan Chen, Qiang Liu, Jialu Chen, Lei Zhang, Tong Cui, Xiaotao Sun, Microstructure and tribological performance of novel Ni-based alloy cladding with excellent high temperature wear resistance and self-lubrication performance, Surf. Coat. Technol. 494 (2024) 131395.
[16] D. Sharma, A. Ameen, A. Alperen Bakir, D. Boruah, E. Davison, K. Wieczerzak, K. Maćkosz, A. Bianchin, S. Paul, Deposition behaviour of FeCrMnNiCo coatings deposited using mechanically alloyed powder: comparing cold spray, HVOF, HVAF, and laser cladding processes, Surf. Coat. Technol. 494 (2024) 131548, https://doi.org/10.1016/j.surfcoat.2024.131548.
[17] R. Kumar, H. Torres, S. Aydinyan, M. Antonov, M. Varga, I. Hussainova, M. Rodriguez Ripoll, Tribological behavior of Ni-based self-lubricating claddings containing sulfide of nickel, copper, or bismuth at temperatures up to 600 °C, Surf. Coat. Technol. 456 (2023) 129270, https://doi.org/10.1016/j.surfcoat.2023.129270.
[18] Qu Cuicui, Xu Bei He, Huaming Wang Cheng, Microstructure and wear characteristics of laser-clad Ni-based self-lubricating coating incorporating MoS2/Ag for use in high temperature, J. Mater. Res. Technol. 33 (2024) 4481–4492, https://doi.org/10.1016/j.jmrt.2024.10.106.
[19] H. Torres, T. Caykara, H. Rojacz, B. Prakash, M. Rodríguez Ripoll, The tribology of Ag/MoS2-based self-lubricating laser claddings for high temperature forming of

aluminium alloys, Wear 442–443 (2020) 203110, https://doi.org/10.1016/j.wear.2019.203110.
[20] X. Shi, Z. Xu, M. Wang, W. Zhai, J. Yao, S. Song, et al., Tribological behavior of TiAl matrix self-lubricating composites containing silver from 25 to 800°C, Wear 303 (2013) 486–494, https://doi.org/10.1016/j.wear.2013.04.009.
[21] S.M. Aouadi, H. Gao, A. Martini, T.W. Scharf, C. Muratore, Lubricious oxide coatings for extreme temperature applications: a review, Surf. Coat. Technol. 257 (2014) 266–277, https://doi.org/10.1016/j.surfcoat.2014.05.064.
[22] H. Torres, S. Slawik, C. Gachot, B. Prakash, M. Rodríguez Ripoll, Microstructural design of self-lubricating laser claddings for use in high temperature sliding applications, Surf. Coat. Technol. 337 (2018) 24–34, https://doi.org/10.1016/j.surfcoat.2017.12.060.
[23] I. Hemmati, V. Ocelík, J.Th.M. De Hosson, Effects of the alloy composition on phase constitution and properties of laser deposited Ni-Cr-B-Si coatings, Phys. Procedia 41 (2013) 302–311, https://doi.org/10.1016/j.phpro.2013.03.082.
[24] X.-B. Liu, C. Zheng, Y.-F. Liu, J.-W. Fan, M.-S. Yang, X.-M. He, M.-D. Wang, H.-B. Yang, L.-H. Qi, A comparative study of laser cladding high temperature wear-resistant composite coating with the addition of self-lubricating WS2 and WS2/(Ni–P) encapsulation, J. Mater. Process. Technol. 213 (2013) 51–58, https://doi.org/10.1016/j.jmatprotec.2012.07.017.
[25] Mao-Sheng Yang, Xiu-Bo Liu, Ji-Wei Fan, Xiang-Ming He, Shi-Hong Shi, Fu Ge-Yan, Ming-Di Wang, Shu-Fa Chen, Microstructure and wear behaviors of laser clad NiCr/Cr3C2–WS2 high temperature self-lubricating wear-resistant composite coating, Appl. Surf. Sci. 258 (2012) 3757–3762, https://doi.org/10.1016/j.apsusc.2011.12.021.
[26] B. Podgornik, S. Hogmark, J. Pezdirnik, Comparison between different test methods for evaluation of galling properties of surface engineered tool surfaces, Wear 257 (2004) 843–851, https://doi.org/10.1016/j.wear.2004.05.005.
[27] Shu Yan Zhang, E. Compagnon, B. Godin, A.M. Korsunsky, Investigation of martensite transformation in 316L stainless steel, Mater. Today Proc. 2 (2015) 251–260, https://doi.org/10.1016/j.matpr.2015.05.035.
[28] U. Wiklund, I.M. Hutchings, Investigation of surface treatments for galling protection of titanium alloys, Wear 251 (2001) 1034–1041, https://doi.org/10.1016/S0043-1648(01)00730-X.
[29] M.R. Vazirisereshk, A. Martini, D.A. Strubbe, M.Z. Baykara, Solid lubrication with MoS2: a review, Lubricants 7 (2019) 57, https://doi.org/10.3390/lubricants7070057.
[30] F. Czerwinski, Thermal stability of aluminum alloys, Materials 13 (2020) 3441, https://doi.org/10.3390/ma13153441.
[31] Sulfur Spectra – Cr2S3. https://xpsdatabase.com/sulfur-spectra-cr2s3. (Accessed 9 February 2025).
[32] M. Sarkar, N. Mandal, Solid lubricant materials for high temperature application: a review, Mater. Today 66 (2022) 3762–3768, https://doi.org/10.1016/j.matpr.2022.06.030.
[33] A. Erdemir, R.A. Erck, G.R. Fenske, H. Hong, Solid/liquid lubrication of ceramics at elevated temperatures, Wear 203-204 (1997) 588–595, https://doi.org/10.1016/S0043-1648(96)07431-5.
[34] I. Hocaoglu, M.N. Cizmeciyan, R. Erdem, C. Ozen, A. Kurt, A. Sennaroglu, H. Yagci Acar, Development of highly luminescent and cytocompatible near-IR-emitting aqueous Ag2S quantum dots, J. Mater. Chem. 22 (2012) 14674–14681, https://doi.org/10.1039/C2JM31959D.
[35] Bingsen Jia, Xu Wenju, Xiaohong Liu, Li Ji, Jia Li, Chufeng Sun, Hongxuan Li, Element diffusion behaviors at high temperature and their effects on microstructure and tribological properties of Cr2O3 films, Appl. Surf. Sci. 613 (2023) 155993, https://doi.org/10.1016/j.apsusc.2022.155993.
[36] S.I. Sadovnikov, A.A. Rempel, A.I. Gusev, Nanostructured Lead, Cadmium and Silver Sulfides: Structure, Nonstoichiometry and Properties, Springer International Publishing AG, Cham/Heidelberg, Germany, 2018, p. 331.
[37] A.A. Valeeva, S.I. Sadovnikov, A.I. Gusev, Polymorphic phase transformations in nanocrystalline Ag2S silver sulfide in a wide temperature interval and influence of nanostructured Ag2S on the interface formation in Ag2S/ZnS heteronanostructure, Nanomaterials 12 (2022) 1668, https://doi.org/10.3390/nano12101668.

Further reading

[38] B. Podgornik, V. Yarasu, B. Šetina Batič, M. Rodriguez Ripoll, Dataset for a Publication "High Temperature Anti-galling Performance of Self-lubricating Ni-based Coatings by Laser Metal Deposition" (Version V1), Zenodo, 2025. https://doi.org/10.5281/zenodo.18015577.